

Temperature Dependent Reverse Recovery Characterization of SiC MOSFETs Body Diode for Switching Loss Estimation In a Half-Bridge

Debiprasad Nayak, *Student Member, IEEE*, Yakala Ravi Kumar, *Student Member, IEEE*,
Manish Kumar, *Student Member, IEEE*, Sumit Pramanick, *Member, IEEE*

Abstract—In a hard switched MOSFET based converter, turn-on energy losses is predominant in the total switching loss. At higher junction temperature the turn-on energy loss further increases due to the reverse recovery effect of the complementary MOSFETs body diode in a half-bridge configuration. Estimation of the switching loss under different operating conditions at an early design stage is essential for optimising the thermal design. Analytical switching loss models available in literature are generally used for estimating the switching losses, due to its accuracy and simplicity. In this paper, the inaccuracy in the reported loss models due to non inclusion of temperature dependent reverse recovery characteristics of body diode, is investigated. A structured method to determine the temperature-dependent switching loss of a SiC MOSFET in a half-bridge is presented. A simple methodology has been proposed to analyze the carrier lifetime's temperature dependencies of a SiC MOSFETs body diode. Device parameters from a 1.2kV/36A SiC MOSFETs datasheet are used for developing the loss model and experimental validation of the model.

Index Terms—SiC MOSFET, temperature, half-bridge, reverse recovery, switching loss, double pulse test.

I. INTRODUCTION

SILICON carbide (SiC) MOSFETs have increasingly become popular as a replacement for Silicon (Si) based insulated gate bipolar transistors (IGBTs) due to its superior physical and electrical characteristics [1], [2]. Despite the improved performance, switching and conduction losses are the major loss contributor in a power semiconductor device. The efficiency of power conversion further reduces at high ambient temperature, as the junction temperature (T_j) increases with the increment of heatsink temperature ($T_{h,s}$), which is common in automotive and grid-connected converters. The maximum ambient temperature in such applications typically ranges from 40°C to 50°C for grid-connected converters and 85°C to 100°C for automotive-grade converters. Therefore, an accurate estimation of semiconductor losses in such high temperature environment is essential for evaluating the efficiency and optimizing the cooling system for overall power density improvement. This work's primary focus is to model and accurately estimate the temperature-dependent switching losses of SiC MOSFETs in a half-bridge, which is the most commonly used building block for DC-DC/DC-AC converters.

In the overall loss of a converter, the conduction loss can be calculated using the temperature-dependent parameter (R_{DS}), available in the datasheet. To accurately estimate the switching losses, different approaches are described in the literature [3].

Among these, the most commonly used methods are physics-based models, numerical models, behavioural model and analytical models. In physics-based models, physical device data for SPICE modelling and field expertise are necessary [4], [5]. Though physical models are accurate enough, it is hindered by the fact that many of its physical parameters are not present in the manufacturer datasheet. In numerical models, simulation tools like SILVACO and TCAD are being used. These simulation tools provide very accurate results, but these tools require material properties, device geometry and are very computationally intensive [6]. Behavioural models are the simplest model, and its solution is dependent on a couple of nonlinear equations which are based on curve fitting parameters [7], [8]. In analytical models, device characteristics are divided into different segments, and governing equations are being derived and parameterized based on datasheet parameters [9]–[11]. In this work, the model presented is a combination of both behavioural and analytical model.

The main problem in estimating the switching losses comes from the modelling of the non-linear parasitic capacitances and the temperature-dependent reverse recovery loss of MOSFETs. Efforts have been made in [11], [12] to consider the non-linearity of the junction capacitance either by two-point or multi-point approximation through curve fitting approach. A voltage-dependent capacitor model is derived in [10], [13] and a charge equivalent capacitance model is given in [9] to reduce the models' complexity. Though many methods are present in the literature, the effect of temperature on reverse recovery loss is not taken in to account for calculating the total loss of the MOSFETs. So at the higher ambient temperature, the above mentioned analytical techniques become erroneous.

In this paper, the analytical model proposed in [9] has been improvised by including temperature dependencies. Estimation of turn-on loss has been emphasized more, as the increase in turn-off loss due to increment of temperature is negligible. The reverse recovery current due to the SiC MOSFETs body diode increases with the rise in T_j due to the dependencies of charge carrier lifetime on temperature. Hence the temperature dependencies of the carrier lifetime and the drift region time constant has been considered and the parameter extraction process for these time constants has been described. Further the impact of parasitic capacitance on the reverse recovery process of the body diode has been discussed. During the switching transition, dV_{ds2}/dt and dI_{d2}/dt of the device under test (DUT) are considered to be linear.

This paper is structured as follows. Section II describes the model parameters used, and Section III describes the switching segments during turn-on with the effect of temperature on reverse recovery of the SiC MOSFETs body-diode. Section IV describes the experimental set-up and discusses experimental and analytical results. Section V concludes the paper.

II. MODEL PARAMETERS

In the conventional MOSFETs loss estimation technique, a closed-form solution with a linear approximation of voltage and current is given for easy calculation [14]–[16]. However, this method does not consider the effect of circuit parasitics and temperature, which results in inaccurate estimation of losses. Given the high switching rate of the SiC MOSFETs, consideration of the effect of parasitics and temperature becomes crucial to remove these inaccuracies. This section introduces to the circuit parasitics and the data extraction process from device datasheet for describing the governing equations during the switching intervals of the DUT.

A. Passive Parameters

The circuit diagram, considering its parasitics, is shown in Fig. 1. The resistances included in this model are gate resistance R_g and parasitic resistance present in the DC bus R_b . The R_b considered here is the resistance from the nearest DC link capacitor to the switches which is the summation of positive rail DC bus resistance $R_{b,1}$ and negative rail DC bus resistance $R_{b,2}$. While switching, the damping for the V_{ds} and I_d oscillations depends on R_b . The parasitic inductances present in the circuit are L_b , L_d and L_s . L_b is the DC bus inductances which consists of $L_{b,1}$ and $L_{b,2}$. L_d , L_s are the drain and source lead inductances of the SiC MOSFETs, respectively. The parasitic capacitances considered in this model are the gate-source capacitance C_{gs} , drain-source capacitance C_{ds} , gate-drain capacitance C_{gd} of the SiC MOSFETs and the load capacitance C_L .

Typically the capacitances values provided in the device datasheets are input, output and reverse transfer capacitances

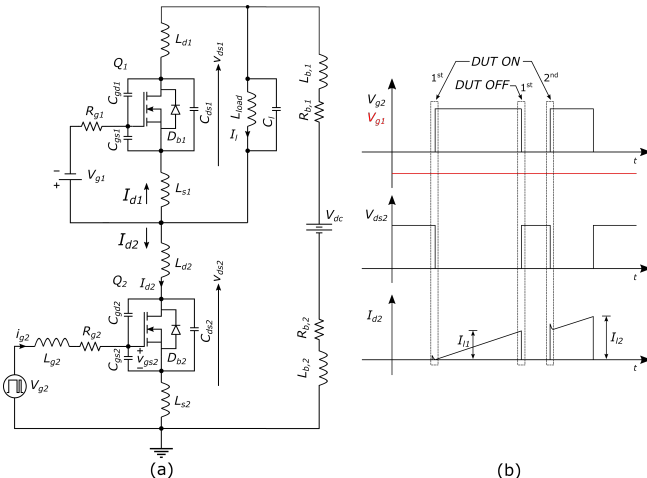


Fig. 1: (a) Double pulse test circuit with circuit parasitics and (b) Switching waveforms in double pulse test

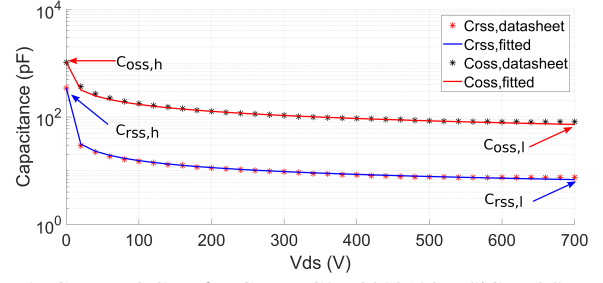


Fig. 2: C_{oss} and C_{rss} for CREE C2M0080120D SiC MOSFET and their fitted curves

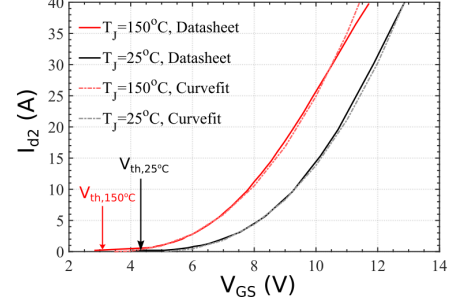


Fig. 3: Transconductance (g_m) characteristics of SiC MOSFET C2M0080120D

(C_{iss} , C_{oss} and C_{rss}) which are voltage dependent and can be modelled as per eq. 1 [10], and the average charge equivalent capacitances can be determined as per eq. 2

$$C_x(V_{ds}) = \frac{C_{o,x}}{\sqrt{(1 + \frac{V_{ds}}{a_x}) + b_x}} \quad (1)$$

$$C_{x,av} = \frac{1}{V_{DC}} \int_0^{V_{DC}} C_x(v_{ds}) dv_{ds} \quad (2)$$

where : $x = iss, oss, rss$

$C_{o,x}$ is the capacitance value at V_{ds} equals to zero. a_x and b_x can be found out by fitting the capacitance (C_x vs V_{ds}) curves provided in datasheet [17]. C_{iss} need not be fitted as its value remains almost constant with respect to V_{ds} and can be directly taken from the datasheet. Fig. 2 shows the fitted curve of C_{oss} and C_{rss} of C2M0080120D SiC MOSFET [17]. From these capacitances the MOSFETs terminal capacitances can be calculated as:

$$\begin{aligned} C_{gs} &= C_{iss} - C_{rss} \\ C_{ds} &= C_{oss} - C_{rss} \\ C_{gd} &= C_{rss} \end{aligned} \quad (3)$$

B. Transfer Equation

During switching transition, the MOSFETs mainly operates in three regions: 1) cut-off region, 2) saturation region and 3) ohmic region. For estimating the switching energy loss of the MOSFET, channel current i_{ch} during saturation region is considered.

In the saturation region the transfer characteristics of a MOSFET is given in its datasheet for a given temperature and can be expressed per eq. 4. The current transconductance factor g_m depends on i_{ch} , and can be expressed as per eq. 5

[18]. Due to the dependency on temperature, g_m changes as T_j increases Fig. 3. The effect of T_j on V_{th} can be expressed as per eq. 6.

$$i_{ch} = k_1[v_{gs} - V_{th}(T_j)]^x + k_2 \quad (4)$$

$$g_m(i_{ch}) = \sqrt[x]{\frac{k_1 i_{ch}^x}{i_{ch} - k_2}} \quad (5)$$

$$V_{th}(T_j) = aT_j^2 + bT_j + c \quad (6)$$

Here a , b , c , k_1 , k_2 and x are the curve-fitting parameters. The values of these parameters are 29×10^{-6} , -15×10^{-3} , 4.9 , 195×10^{-3} , 0 and 2.5 respectively for C2M0080120D.

III. SWITCHING CHARACTERIZATION AND DISCUSSION

This section introduces the switching process of the MOSFETs (Q_1 and Q_2) in a half-bridge configuration represented in Fig. 1(a). The lower MOSFET Q_2 is considered as the DUT.

The double-pulse test (DPT) has been divided into three parts as per Fig. 1(b). At the first turn-on event the voltage across Q_1 , Q_2 are zero and V_{dc} respectively. When the Q_2 is being turned on the parasitic capacitance $C_{oss,2}$ of Q_2 discharges and the $C_{oss,1}$ of Q_1 charges. The current that flows through the MOSFETs in the first turn-on event is due to the MOSFET's parasitic capacitances, which experiences a dV_{ds}/dt across it. At the first turn-off event of Q_2 , I_{d2} starts to fall and V_{ds2} starts to rise while charging its $C_{oss,2}$. The load current I_{load} starts to transfer to the body-diode of Q_1 and V_{ds1} starts to fall while discharging its $C_{oss,1}$. In the second turn-on event of Q_2 , I_{load} starts transferring from Q_1 to Q_2 and during this, in addition to the capacitive current, reverse recovery current of Q_1 increases the turn-on loss of Q_2 . This turn-on loss increases significantly with the increase in T_j due to reverse recovery current of the body diode of Q_1 , which has been explained in Section III-B.

A. Turn-On Transient

Under hard switching conditions, contribution of turn-on loss E_{on} in the total MOSFET switching loss E_{tot} is significant. However, E_{on} increases as T_j increases, so the effect of temperature must be included in the loss estimation. A detailed interval wise turn-on process can be seen from Fig. 4.

1) *Interval 0 (Delay Time)*: This stage starts with increase in gate voltage $V_{gs,2}$ from negative gate bias voltage V_{EE} to threshold voltage V_{th} with a time constant of $R_g(C_{gs} + C_{gd,h})$. This interval is known as turn-on delay time $t_{d,on}$. In this interval as $V_{gs,2}(t) < V_{th}$, there is no drain current I_{d2} in MOSFET Q_2 and all the I_{load} flows through the body diode of MOSFET Q_1 . The voltage across the $V_{ds,2}$ remains at $V_{dc} + V_{fd1}$.

$$v_{gs}(t) = V_{CC} + [V_{EE} - V_{CC}]e^{-\frac{t}{R_g(C_{gs} + C_{gd,h})}} \quad (7)$$

$$T_0 = R_g(C_{gs} + C_{gd,h}) \ln \frac{V_{CC} - V_{EE}}{V_{CC} - V_{th}(T_j)}$$

$$E_{on,0} = 0$$

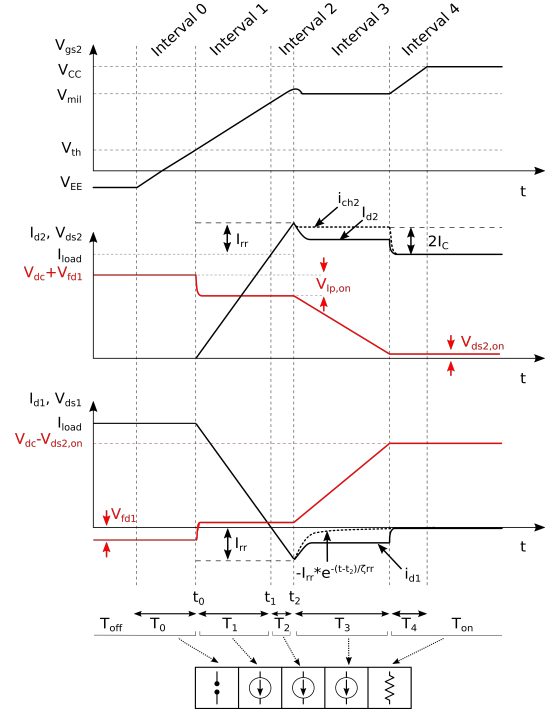


Fig. 4: Turn-on process MOSFET Q_1 and Q_2 in a half bridge

2) *Interval 1 (Current Rise Time)*: In this interval as $v_{gs}(t)$ crosses the V_{th} , Q_2 channel current I_{ch2} starts to rise to I_{load} . In this interval I_{d2} remains equal to I_{ch2} and the V_{ds2} drops to $V_{dc} + V_{fd1} - V_{Lp,on}$. Voltage $V_{Lp,on}$ is the addition of voltage drops across L_b , L_{d2} and L_{s2} . The dynamics of the gate voltage, time duration and the energy loss in this interval are expressed in eq. 8. The dV_{gd}/dt and dV_{ds}/dt does not change significantly in this interval, so for simplicity, these can be assumed to be zero.

$$v_{gs}(t) = V_{CC} + [V_{th}(T_j) - V_{CC}]e^{-\frac{t}{R_g C_{gs} + L_s g_m(T_j)}}$$

$$T_1 = \left| - (R_g C_{gs} + L_s g_m(T_j)) \ln \left(1 - \frac{I_{load}}{g_m(T_j)(V_{CC} - V_{th}(T_j))} \right) \right|$$

$$V_{Lp,on} = L_p \frac{I_{load}}{t_{1,2}}$$

$$E_{on,1} = \frac{1}{2} T_1 (V_{dc} + V_{fd1} - V_{Lp,on}) I_{load} \quad (8)$$

3) *Interval 2 (Storage Time)*: At this interval I_{d2} continues to rise above I_{load} to $I_{load} + I_{rr}$. Due to the reverse recovery of MOSFET Q_1 , V_{ds2} stays at $V_{dc} + V_{fd1} - V_{Lp,on}$. The circuit condition does not change from interval 1, but the time duration T_2 changes with respect to the I_{load} and T_j . The detailed working process of MOSFETs body diode in this interval with I_{load} and T_j dependencies is explained in Section III-B. The energy loss of Q_2 in this interval can be expressed as eq. 9.

$$E_{on,2} = (V_{dc} + V_{fd1} - V_{Lp,on})(I_{load} + \frac{1}{2} I_{rr}) T_2 \quad (9)$$

4) *Interval 3 (Voltage Fall Time)*: After the current $I_{d1}(t)$ in the body diode of MOSFET Q_1 reaches to I_{rr} , it starts to block the voltage V_{ds1} across it and simultaneously the

V_{ds2} across Q_2 starts to fall. Here as V_{ds1} starts to rise, the parasitic capacitance C_{oss1} starts to charge and the parasitic capacitance C_{oss2} starts to discharge. The charging current of C_{oss1} is termed as I_{C1} and the discharging current of C_{oss2} is termed as I_{C2} . Due to C_{gd1} discharging, the voltage V_{gs2} in this interval stays at miller plateau voltage V_{mil} . The net current which flows through the channel of MOSFET Q_2 is $I_{ch2} = I_{load} + I_{C1} + I_{C2} + I_{rr}e^{-(t-t_2)/\tau_{rr}}$ (details about τ_{rr} is given in Section III-B). If both the MOSFET Q_1 and Q_2 are same then the parasitic capacitance across it can be considered to be same, so $I_{C1}=I_{C2}=I_C$. For calculating the energy loss in this interval, i_{ch} has been divided in to two parts: first is due to $I_{load} + 2I_C$ and the second is due to $I_{rr}e^{-(t-t_2)/\tau_{rr}}$. The capacitive current I_C can be found from the quadratic equation given in [9] as:

$$I_C = \left| \frac{-B_1 + \sqrt{B_1^2 - 4A_1C_1}}{2A_1} \right| \quad (10)$$

where:

$$A_1 = \frac{-2L_s}{Q_C R_g}$$

$$B_1 = \frac{C_{gd,av}}{C_{gd,av} + C_{ds,av}} + \frac{2}{g_m(T_j)R_g}$$

$$C_1 = \frac{V_{CC} - V_{th}(T_j)}{R_g} - \frac{I_{load}}{R_g g_m(T_j)}$$

I_C is being determined through numerical iterative method, as g_m changes according to i_{ch} and T_j . So the iteration process will continue until the error in the calculation of I_C becomes negligible. Q_C is the net charge stored in the parasitic output capacitances of Q_1 or Q_2 (as the identical MOSFETs will have same charge storing capacity) and can be written as eq. 11. The duration in which V_{ds2} fall depends on the effective discharging time of the parasitic capacitance and is given as eq. 12.

$$Q_C = V_{dc}C_{oss2,av} \quad (11)$$

$$T_3 = \frac{Q_C}{I_C} \quad (12)$$

The total energy loss in the MOSFET Q_1 in this interval can be written as

$$E_{on,3} = \frac{1}{2}(I_{load} + 2I_C)(V_{dc} + V_{fd1} - V_{Lp,on} - V_{ds2,on})T_3$$

$$+ (I_{load} + 2I_C)V_{ds2,on}T_3$$

$$+ \tau_{rr}I_{rr}[(V_{dc} + V_{fd1} - V_{Lp,on})(1 - e^{-T_3/\tau_{rr}})]$$

$$+ \tau_{rr}I_{rr}(V_{ds2,on} - V_{dc} - V_{fd1} + V_{Lp,on})$$

$$[(\tau_{rr}/T_3)(1 - e^{-T_3/\tau_{rr}}) - e^{-T_3/\tau_{rr}}] \quad (13)$$

5) *Interval 4*: This interval starts when MOSFET Q_2 enters from saturation region to ohmic region. The gate voltage V_{gs2} starts rising from V_{mil} to V_{CC} and the V_{ds2} remains at $V_{ds2,on}$, hence this interval can be neglected from the switching interval. The energy loss in this interval can be approximated as $E_{on,4} \approx V_{ds2,on}I_{d2}T_4$, where $T_4 \approx 2R_g(C_{gs} + C_{ds2,l})$. From

the five turn-on switching intervals, interval 0, 4 remains in the cutoff and ohmic regions. In interval 1, 2 and 3, the SiC MOSFET remains in saturation as in this interval $V_{gs} > v_{th}$ and $V_{ds} > v_{gs} - V_{th}$. Therefore for calculating the total turn-on energy loss, switching intervals 1, 2 and 3 are being considered and can be written as:

$$E_{on,tot} = E_{on,1} + E_{on,2} + E_{on,3} \quad (14)$$

B. Reverse Recovery Loss Model

This section describes the reverse recovery process of the body diode of the SiC MOSFET. The time period during this mode increases with respect to T_j and I_{load} . So to estimate this duration, the power diode model from [19], [20] has been improved for better accuracy under different T_j and further the impact of displacement current from parasitic capacitance has been discussed. For developing a comprehensive MOSFETs body diode model, the behaviour of the body-diode during turn-off needs to be analysed first. Fig. 5(a) shows the behaviour of a 36A/1.2kV SiC MOSFETs body diode during turn-off at different T_j .

The reverse recovery process starts when the current through the diode starts to flow in the negative direction. The rate at which body-diode current $I_{d1}(t)$ falls below zero, dI_{d1}/dt depends on the circuit stray inductance L_p and the applied reverse bias voltage V_{ds1} across the MOSFET. As the diode current enters into the negative region, the excess charge carriers present in the junction starts to reduce while the I_{d1} starts to fall towards the negative peak of the reverse recovery current I_{rr} . This region from t_1 to t_2 termed as storage phase. After the excess charge carriers become zero at t_2 , depletion region starts to form and the reverse voltage across the diode starts to rise at the rate of dV_{ds1}/dt . Time period from t_2 to t_3 is termed as recovery phase (Fig. 6).

After t_2 , as V_{ds1} starts rising towards $V_{dc} - V_{ds2,on}$, parasitic capacitance across the body-diode $C_j = C_{oss1} + C_l$ begins to charge and capacitive displacement current $I_{cj}(t)$ starts to flow. The magnitude of $I_{cj}(t)$ depends on the rate of dV_{ds1}/dt . Time duration from t_2 to t_4 is termed as the voltage-rise phase. The reverse-recovery characteristics in the voltage-rise phase depends upon two currents: actual body-diode reverse recovery current due to the depletion region formation $I_{bd}(t)$ and $I_{cj}(t)$. After t_4 , $I_{d1}(t)$ reaches to its leakage current I_{lk} level. The $I_{bd}(t)$ during the entire reverse-recovery phase can be written as per eq. 15.

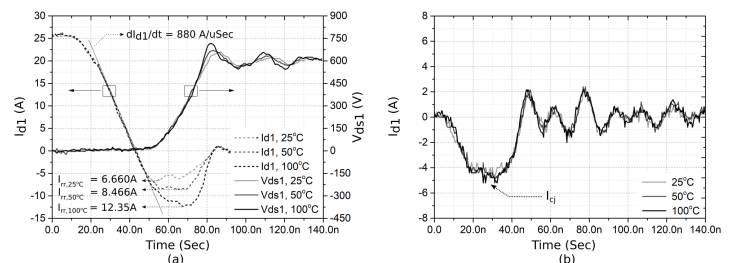


Fig. 5: (a) Reverse recovery of C2M0080120D at different T_j and (b) The capacitive displacement current $I_{cj}(t)$ of Q_1 under different T_j at 1st DUT on instance

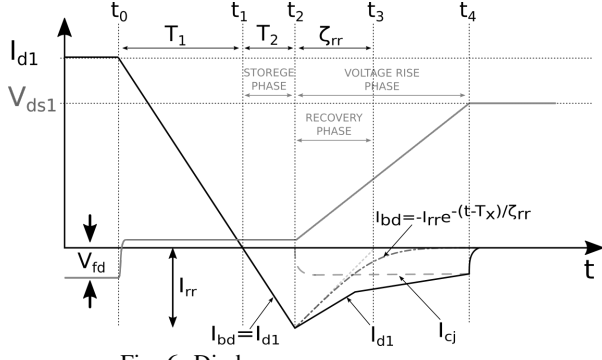


Fig. 6: Diode reverse recovery process

$$I_{bd}(t) = \begin{cases} I_{load} - \frac{V_{ds1} t}{L_s}, & t < t_2 \\ -I_{rr} e^{-\frac{(t-t_2)}{\tau_{rr}}} - I_{cj}(t), & t_2 \leq t \leq t_4 \\ I_{lk} \approx 0, & t \geq t_4 \end{cases} \quad (15)$$

To further describe the dynamics of the body diode and to find out I_{rr} for any operating conditions, three time constants are introduced as [19]: drift region transit time T_m , charge carrier life time τ_c and time constant of decay fall τ_{rr} . These are inter related as per eq. 16. From these time constants, I_{rr} can be calculated by solving eq. 17 numerically for T_2 .

$$\frac{1}{\tau_{rr}} = \frac{1}{\tau_c} + \frac{1}{T_m} \quad (16)$$

$$T_m \left[I_{load} - \frac{I_{load}}{T_1} (T_1 + T_2) \right] = \frac{I_{load}}{T_1} \tau_c \left[-T_2 + \tau_c - \tau_c e^{-\frac{-(T_1 + T_2)}{\tau_c}} \right] \quad (17)$$

As the T_j increases, these time constants tends to change. Hence the proposed extraction method in [19] to find out I_{rr} is not applicable for varying T_j . So an equivalent reverse recovery charge model is presented to find out the time period T_2 . The total reverse recovery charge Q_{rr} is calculated as per eq. 18. This Q_{rr} combines both the reverse recovery charge Q_{rr}^* , which is due to $I_{bd}(t)$ and the capacitive charge Q_{cj} due to $I_{cj}(t)$ through parasitic capacitance C_j . As T_j increases, the magnitude of I_{rr} increases. Due to I_{rr} , Q_{rr}^* also increases, but the Q_{cj} remains constant, as $I_{cj}(t)$ does not change with respect to temperature Fig. 5(b).

$$Q_{rr} = \int_{I_{d1}(t) < 0} I_{bd}(t) dt \quad (18)$$

$$Q_{rr} = Q_{rr}^* + Q_{cj} \quad (19)$$

$$I_{d1}(t) = I_{bd}(t) + I_{cj}(t) \quad (20)$$

$I_{cj}(t)$ can be approximated as per eq. 21 [21], which remains constant for period T_3 time period. The capacitive charge Q_{cj} can be found out from the first turn-on instant of DUT as per Fig. 5(b) by finding the area under the curve or from the datasheet parameters as per eq. 21. At this instant the

net Q_{rr} is only due to Q_{cj} , as the $I_{d1}(t)$ prior to this instant is zero. From Fig. 5(b) Q_{cj} can be experimentally calculated as per eq. 18.

$$I_{cj}(t) = C_j \frac{dV_{ds1}}{dt} \quad (21)$$

$$Q_{cj} = \int_{t_2}^{t_4} I_{cj}(t) dt$$

To find out the temperature dependencies of Q_{rr} , DPT at different T_j needs to be performed, from which Q_{rr}^* can be calculated as per eq. 19. In some manufacturer datasheet Q_{rr} at two temperature are given which can be directly used to find out Q_{rr}^* . The time constant of decay fall τ_{rr} only depends on the I_{rr} , and the relationship between τ_{rr} and Q_{rr}^* can be written as eq. 22. Here it is assumed that after τ_{rr} time, the contribution of $I_{bd}(t)$ in $I_{d1}(t)$ is negligible as per Fig. 6.

$$Q_{rr}^* = 0.5 * I_{rr} \left(\frac{1}{dI_{d1}/dt} I_{rr} + \tau_{rr} \right) \quad (22)$$

To determine the τ_c , τ_m and τ_{rr} for any arbitrary operating conditions eq. 16, eq. 23 and eq. 24 need to be solved numerically.

$$I_{rr} = \frac{1}{2 \cdot dI_{d1}/dt} (\tau_c - \tau_{rr}) \left(1 - e^{-T_1/\tau_c} \right) \quad (23)$$

$$\frac{I_{rr}}{dI_{d1}/dt} (\tau_c + T_m) = \tau_{rr}^2 \left(1 - e^{-T_1/\tau_c} \right) \quad (24)$$

IV. RESULTS AND DISCUSSION

A. Experimental Setup

To study the effect of reverse recovery and switching energy loss at high T_j , the DPT has been carried out at 600V DC bus voltage and load current till 25A. The experimental results are taken for the validation of the temperature dependent loss model proposed in this paper. A SiC MOSFET C2M0080120D rated at 1200V and 36A [17] is used for the half-bridge in the DPT setup.

For the gate-driver circuit, an isolated DC-DC converter with an output of +20/-5V and an optoisolator ACPL-337J are used. A total of 9.98Ω resistance is used as gate resistance R_g for the MOSFETs. Low ESL DC link capacitors are being used near the half-bridge to reduce the DC bus inductance. A single layer air core inductor with an inductance of 475μH is used as a load inductor.

A passive differential voltage probe (MDO3104) and a current probe (TCP0030A) from Tektronix are being used to measure the switching voltage and current transients. The heatsink was preheated before conducting the DPT at different temperatures until it reached a thermal equilibrium state to measure the switching performance. It is assumed that, under the thermal equilibrium state, the T_j is equal to the T_{hs} . T_{hs} is continuously monitored by a thermocouple temperature probe Fluke 80BK-A, and to further increase the accuracy of the reading, infrared thermal camera Flir E63900 is being used Fig. 7.

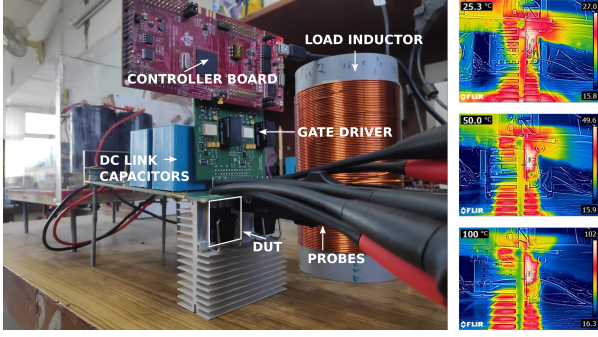


Fig. 7: Experimental test set-up with thermal images ($T_{hs} = 25^\circ C, 50^\circ C$ and $100^\circ C$) of the DUT

Switching energy loss estimation is very sensitive to voltage-current timing misalignment. The propagation delay between the two probes is known as skew. So for accurate measurement, voltage and current probes need to be properly de-skewed. A resistive DPT has been conducted with a low inductive 30Ω resistor to verify the propagation delay time for each measuring probes.

B. Parameter Extraction

The parameters used in the loss model are extracted from the SiC MOSFETs datasheet and from the experimental results.

For calculating the transconductance $g_m(i_{ch})$, curve fit values based on the transfer characteristics from the datasheet of C2M00801120D are being used as per eq. 5. The datasheet and the fitted curves at two different T_j are shown in Fig. 3. It can be seen that as the T_j increases from $25^\circ C$ to $150^\circ C$, V_{th} decreases from $4.5V$ to $3.3V$.

For extracting the non-linear capacitance values, eq. 1 is used to find out the average capacitance values for saturation region. The maximum and minimum values of the capacitances are used for ohmic, cutoff regions, respectively. The curve fitting parameters and the extracted values are tabulated in Table I and II.

The DC bus inductance is calculated from the voltage drop $V_{Lp,on}$ in V_{ds2} due to the parasitic inductances from the turn-on switching waveform as shown in Fig. 9(h). The total path inductance is found out to be $66.21nH$ as per eq. 8. The influence of L_{s2} is more on the switching transients and hence needs to be subtracted from the total path inductance and considered separately. In this work the value of L_{s2} is considered to be $9nH$ [22], [23].

The extraction of fitting parameters for Q_{rr} and Q_{rr}^* are done at $T_j = 25^\circ C, 50^\circ C$ and $100^\circ C$. The operating conditions are $V_{dc} = 600V$ and $I_{d1} = 25A$. Further to see the effect of load current on dI_{d1}/dt during the fall time, I_{d1} is varied from $0A$ to $25A$ as per Fig. 9(a),(b) and (c). From all the test conditions, it is observed that dI_{d1}/dt approximately remains constant at $880A/\mu s$. It can be observed from Fig. 9(a), at lower temperature ($T_j = 25^\circ C$), during the storage phase the change in dI_{d1}/dt is not significant with respect to load current. However, at higher temperature ($T_j = 50^\circ C$ and $100^\circ C$) it can be observed from Fig. 9(b) and (c), that dI_{d1}/dt does not remain constant throughout the storage phase with respect to load current and tends to change before it reaches to

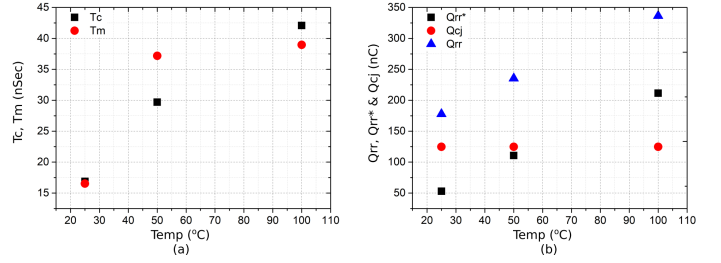


Fig. 8: (a)Variation of T_m and τ_c with respect to temperature (T_j) and (b)Variation of Q_{rr} , Q_{rr}^* and Q_{cj} with respect to temperature (T_j)

TABLE I: Capacitance Curve Fitting Parameters

Capacitance	$C_{o,x}$	a_x	b_x
C_{oss}	1040 pF	3	1.25
C_{rss}	344.2 pF	0.19	1.25

TABLE II: Non Linear Capacitances

Conditions	$v_{gs} < V_{th}$ $V_{ds} \geq v_{gs} - V_{th}$ Cutoff	$v_{gs} > V_{th}$ $V_{ds} > v_{gs} - V_{th}$ Saturation	$v_{gs} > V_{th}$ $V_{ds} \leq v_{gs} - V_{th}$ Ohmic
C_{gd}	$C_{gd,l} = 8pF$	$C_{gd,av} = 12pF$	$C_{gd,h} = 500pF$
C_{ds}	$C_{ds,l} = 72pF$	$C_{ds,av} = 111pF$	$C_{ds,h} = 540pF$

TABLE III: Curve Fitting Parameters From Reverse Recovery Test

Parameters	α	β	γ	m	c
$\tau_c(nSec)$	-447.6	-0.04924	398.9	-	-
$T_m(nSec)$	-2.074e6	-3.55	39.12	-	-
$Q_{rr}(nC)$	-	-	-	2.101	127.3
$Q_{rr}^*(nC)$	-	-	-	2.101	2.54

peak reverse recovery current (I_{rr}). The change in the dI_{d1}/dt during storage phase is termed as dI_{d1}^1/dt , and it increases with respect to T_j . Further as per Fig. 5(a), at higher T_j , V_{ds1} starts to rise before the body-diode current reaches to I_{rr} . This phenomena increases the reverse recovery loss at a higher temperature. For simplicity in this work, it is assumed that V_{ds1} rises after the I_{rr} reaches to its peak at t_2 as shown in Fig. 6.

The body-diode's time constants τ_c and T_m are found out as per the discussion in Section III-B and are shown in Fig. 8(a). The increment in τ_c and T_m with respect to T_j increases rapidly at lower temperature range but tends to reduce at higher temperature Fig. 8(a). The change in Q_{rr} , Q_{rr}^* and Q_{cj} with respect to temperature is shown in Fig. 8(b). The dynamics of τ_c and T_m and Q_{rr}^* from the experimental results can be expressed as per eq. 25 and 26:

$$\begin{aligned} \tau_c(nSec) &= \alpha_1 T_j^{\beta_1} + \gamma_1 \\ T_m(nSec) &= \alpha_2 T_j^{\beta_2} + \gamma_2 \end{aligned} \quad (25)$$

$$\begin{aligned} Q_{rr}(nC) &= m_1 T_j + c_1 \\ Q_{rr}^*(nC) &= m_2 T_j + c_2 \end{aligned} \quad (26)$$

The fitting parameters for the above equations are given in Table III.

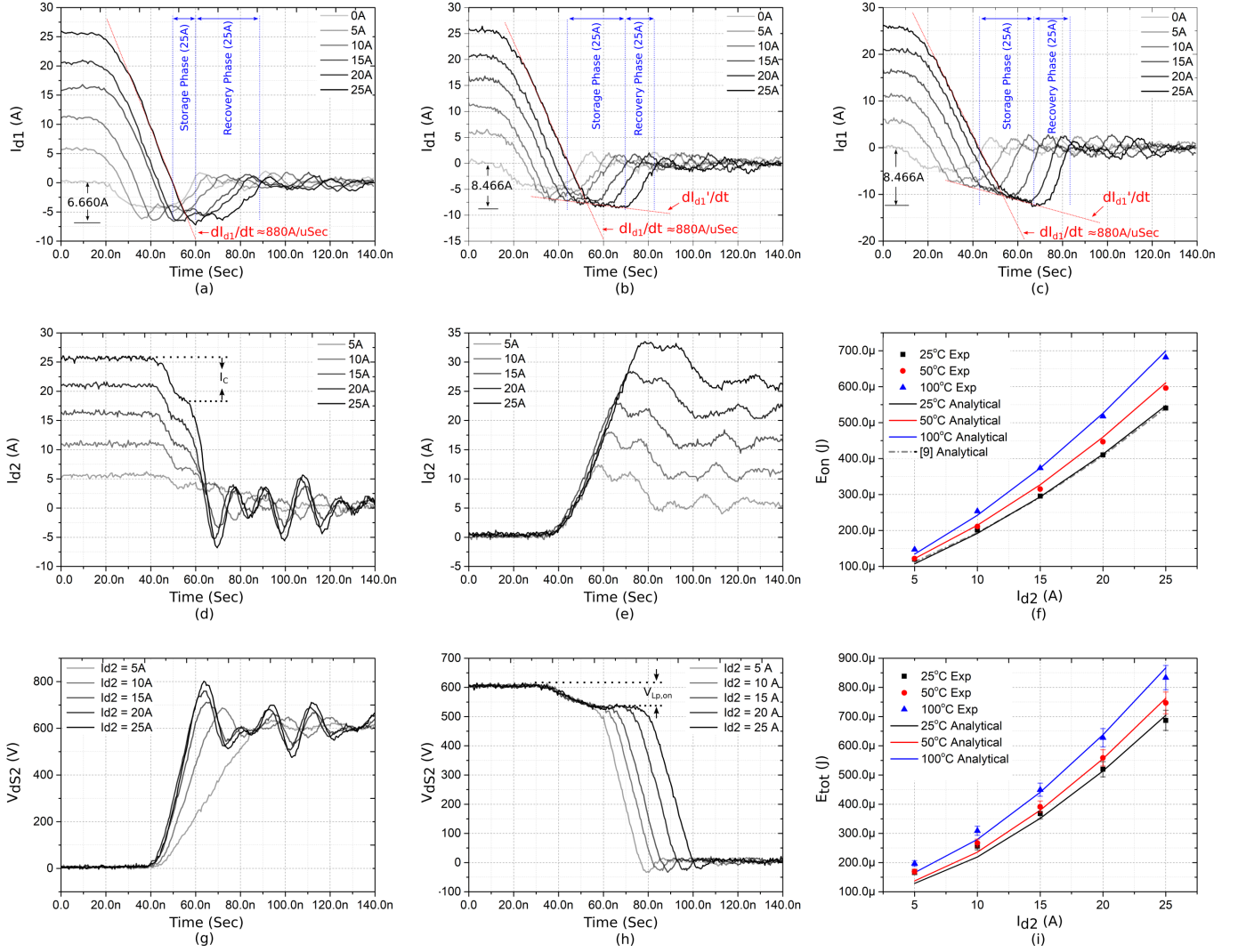


Fig. 9: (a)Reverse recovery current I_{d1} at 25°C , (b)Reverse recovery current at $I_{d1}(t)$ at 50°C , (c)Reverse recovery current at $I_{d1}(t)$ at 100°C , (d) I_{d2} fall transition at $T_j = T_{hs} = 25^{\circ}\text{C}$, (e) I_{d2} rise transition at $T_j = T_{hs} = 25^{\circ}\text{C}$, (f)Turn on energy loss at $T_j = T_{hs} = 25^{\circ}\text{C}$, 50°C and 100°C , (g) V_{ds2} rise transition at different load current under $T_j = T_{hs} = 25^{\circ}\text{C}$, (h) V_{ds2} fall transition at different load current under $T_j = T_{hs} = 25^{\circ}\text{C}$, (i)Total energy loss at $T_j = T_{hs} = 25^{\circ}\text{C}$, 50°C and 100°C

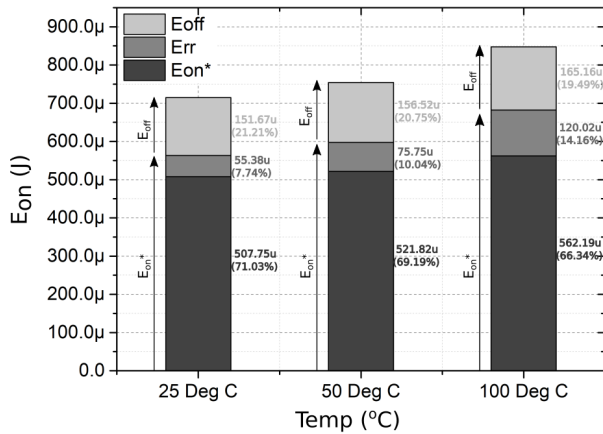


Fig. 10: Analytical energy loss segments under $T_j = 25^{\circ}\text{C}$, 50°C and 100°C for $V_{dc} = 600\text{V}$ and $I_{load} = 25\text{A}$

C. Energy Loss Verification

The loss estimation model presented in Section III is used for computing the turn-on energy losses at different operating temperatures ($T_j = 25^{\circ}\text{C}$, 50°C and 100°C). The experimental energy losses are calculated by multiplying the V_{ds2} and I_{d2} during switching (Fig. 9(e) and (h) for turn-on and Fig. 9(d) and (g) for turn-off), and calculating the area under the curve. The analytical and experimental results of turn-on loss and total switching loss are compared and plotted in Fig. 9(f) and (i) respectively. Over a wide operating range the maximum and minimum error in the estimation of E_{on} are +4.0% and -10.86% respectively. From Fig. 9(f) it can be observed that, due to the inclusion of temperature dependent SiC MOSFETs body-diode time constants, the proposed model's accuracy for E_{on} calculation significantly increases at higher T_j compared to the loss model in [9]. The loss model in [9] is used to plot the turn-on loss in Fig. 9(f) under different loading conditions, using device data-sheet parameters which are available only

at $T_j = 25^\circ\text{C}$. It can be observed that due to non-inclusion of temperature dependent variations, the loss model in [9] shows significant error at high temperature. This error has been shown to reduce with the proposed work in this paper.

For calculating the total energy loss E_{tot} , estimation of turn-off energy loss E_{off} is directly included, as per the method given in [9] as E_{off} does not change significantly with respect to T_j . Fig. 10 shows the loss distribution in E_{tot} and the energy loss due to reverse recovery of Q_1 on Q_2 is subtracted from eq. 14 and shown separately as E_{rr} . It can be seen that E_{rr} increases by 116.7%, when T_j is increased from 25°C to 100°C . The absolute maximum and minimum error range in the estimation of E_{tot} are 22.8% and 4.0%, respectively. The error in E_{tot} increases at low value of I_{load} due to the estimation error in E_{off} at $0 \leq I_{load} \leq 2I_C$. At this current level, I_{ch2} of Q_2 becomes zero, due to which, dV_{ds2}/dt and I_{d2}/dt decreases significantly. In the experimental calculation, an accuracy band of $\pm 5\%$ is created for the measurement error introduced by the voltage and current probes.

V. CONCLUSION

In this paper, a combination of an analytical and behavioural model for estimating the temperature-dependent turn-on switching losses of a SiC MOSFET in a half-bridge configuration is presented. The impact of displacement current due to the SiC MOSFETs parasitic capacitance on estimating the reverse-recovery charge of the body-diode has been analysed. The impact of temperature on the carrier lifetime of the body diode has been discussed. A parameter extraction routine has been followed for modelling the SiC MOSFET and its body diode characteristics. Further, the temperature-dependent charge carrier lifetime of SiC MOSFETs' body-diode has been experimentally calculated and used in the turn-on switching loss model. The proposed model can give the segmented analytical expression for turn-on energy losses, including the device non-idealities. For the validation of the model double-pulse test has been conducted at different T_j (25°C , 50°C and 100°C). The experimental and analytical results are compared over a wide operating range, and the absolute error in the estimation of turn-on switching energy loss is found to be 4% to 10.86%, respectively.

REFERENCES

- [1] J. Biela, M. Schweizer, S. Waffler, and J. W. Kolar, "SiC versus Si—Evaluation of Potentials for Performance Improvement of Inverter and DC–DC Converter Systems by SiC Power Semiconductors," *IEEE Trans. Ind. Electron.*, vol. 58, no. 7, pp. 2872–2882, Jul. 2011.
- [2] J. Millan, P. Godignon, X. Perpina, A. Perez-Tomas, and J. Rebollo, "A Survey of Wide Bandgap Power Semiconductor Devices," *IEEE Trans. Power Electron.*, vol. 29, no. 5, pp. 2155–2163, May 2014.
- [3] H. A. Mantooth, K. Peng, E. Santi, and J. L. Hudgins, "Modeling of Wide Bandgap Power Semiconductor Devices—Part I," *IEEE Trans Electron Devices.*, vol. 62, no. 2, pp. 423–433, Feb. 2015.
- [4] R. Kraus and A. Castellazzi, "A Physics-Based Compact Model of SiC Power MOSFETs," *IEEE Trans. Power Electron.*, vol. 31, no. 8, pp. 5863–5870, Aug. 2016.
- [5] S. Potbhare, N. Goldsman, A. Lelis, J. M. McGarrity, F. B. McLean, and D. Habersat, "A Physical Model of High Temperature 4H-SiC MOSFETs," *IEEE Trans Electron Devices.*, vol. 55, no. 8, pp. 2029–2040, Aug. 2008.
- [6] B. N. Pushpakaran, S. B. Bayne, and A. A. Ogunniyi, "Electro-thermal transient simulation of silicon carbide power MOSFET," in *2013 19th IEEE Pulsed Power Conf. (PPC)*. San Francisco, CA, USA: IEEE, Jun. 2013, pp. 1–6.
- [7] P. Alexakis, O. Alatise, L. Ran, and P. Mawby, "Modeling power converters using hard switched silicon carbide MOSFETs and Schottky barrier diodes," in *2013 15th Eur. Conf. Power Electron. Appl. (EPE)*. Lille, France: IEEE, Sep. 2013, pp. 1–9.
- [8] A. Merkert, T. Krone, and A. Mertens, "Characterization and Scalable Modeling of Power Semiconductors for Optimized Design of Traction Inverters with Si- and SiC-Devices," *IEEE Trans. Power Electron.*, vol. 29, no. 5, pp. 2238–2245, May 2014.
- [9] D. Christen and J. Biela, "Analytical Switching Loss Modeling Based on Datasheet Parameters for MOSFETs in a Half-Bridge," *IEEE Trans. Power Electron.*, vol. 34, no. 4, pp. 3700–3710, Apr. 2019.
- [10] S. K. Roy and K. Basu, "Analytical Estimation of Turn on Switching Loss of SiC mosfet and Schottky Diode Pair From Datasheet Parameters," *IEEE Trans. Power Electron.*, vol. 34, no. 9, pp. 9118–9130, Sep. 2019.
- [11] J. Wang, H. S.-h. Chung, and R. T.-h. Li, "Characterization and Experimental Assessment of the Effects of Parasitic Elements on the MOSFET Switching Performance," *IEEE Trans. Power Electron.*, vol. 28, no. 1, pp. 573–590, Jan. 2013.
- [12] Yuancheng Ren, Ming Xu, Jinghai Zhou, and F. Lee, "Analytical loss model of power MOSFET," *IEEE Trans. Power Electron.*, vol. 21, no. 2, pp. 310–319, Mar. 2006.
- [13] X. Wang, Z. Zhao, K. Li, Y. Zhu, and K. Chen, "Analytical Methodology for Loss Calculation of SiC MOSFETs," *IEEE Trans. Emerg. Sel.*, vol. 7, no. 1, pp. 71–83, Mar. 2019.
- [14] R. W. Erickson and D. Maksimovic, *Fundamentals of power electronics*. Springer Science & Business Media, 2007.
- [15] "Efficiency of buck converter," [online] available: www.rohmfs.rohm.com, 2016.
- [16] "An Accurate Approach for Calculating the Efficiency of a Synchronous Buck Converter Using the MOSFET Plateau Voltage," *Texas Instruments*, 2020.
- [17] "C2m0080120d mosfet datasheet," [online] available: <https://www.wolfspeed.com>, 2020.
- [18] R. Perret, "Power electronics semiconductor devices," Jan. 2009.
- [19] P. Lauritzen and C. Ma, "A simple diode model with reverse recovery," *IEEE Trans. Power Electron.*, vol. 6, no. 2, pp. 188–191, Apr. 1991.
- [20] C. L. Ma, P. O. Lauritzen, and J. Sigg, "Modeling of power diodes with the lumped-charge modeling technique," *IEEE Trans. Power Electron.*, vol. 12, no. 3, pp. 398–405, 1997.
- [21] D. Nayak, M. Kumar, and S. Pramanick, "Analysis of switching loss reduction of sic mosfet in presence of antiparallel sic schottky diode," in *2020 IEEE International Conf. Power Electron., Smart Grid and Renewable Energy (PESGRE2020)*, 2020, pp. 1–6.
- [22] L. Zhang, S. Guo, X. Li, Y. Lei, W. Yu, and A. Q. Huang, "Integrated SiC MOSFET module with ultra low parasitic inductance for noise free ultra high speed switching," in *2015 IEEE 3rd Workshop on Wide Bandgap Power Devices and Applications (WiPDA)*. Blacksburg, VA, USA: IEEE, Nov. 2015, pp. 224–229.
- [23] "C2m0080120d silicon carbide power mosfet Itspace model," [online] available: www.wolfspeed.com.